Letter

Asymmetric thermal conductivity mediated by nonreciprocal polaritons

Sina Jafari Ghalekohneh [1] and Bo Zhao [1,2,*]

[1]*Department of Mechanical and Aerospace Engineering, University of Houston, Houston, Texas 77204, USA*

[2]*Department of Physics, University of Houston, Houston, Texas 77204, USA*

(Received 24 October 2025; revised 15 December 2025; accepted 19 December 2025; published 14 January 2026)

As a type of energy carrier, polaritons can play a dominant role in the thermal conductivity of nano/microstructures. Here, we report an asymmetric thermal conductivity mediated by polaritons that break the Lorentz reciprocity. In contrast to existing approaches that rely on nonlinearity or time modulation, we leverage nonreciprocal polaritons induced by magnetic effects. We show that nonreciprocal surface plasmon polaritons in time-reversal symmetry-breaking systems, including magneto-optical materials and magnetic Weyl semimetals, can alter the symmetry of thermal conductivity in systems like thin films, resulting in direction-dependent thermal conductivity. Thermal conductivities of reciprocal material systems can also be made asymmetric through near-field coupling with these material systems. In accompaniment with the surging interest in nonreciprocal thermal radiation by polaritons, we extend the role of nonreciprocal polaritons from radiative heat transfer systems to conduction systems, paving the way for next-generation thermal devices and efficient energy management solutions.

DOI: 10.1103/pplf-ytqm

Introduction. Nonreciprocal or asymmetric thermal conductivity of materials is the key to unlock applications such as thermal diodes [1,2], thermal transistors [3], thermal memory [4], and thermal circuits [5–7]. However, the thermal conductivity of most traditional materials is reciprocal, which is rooted in the fundamental symmetry of the transport properties of the energy carriers in the system [8]. There has been a tremendous research effort towards enabling asymmetric thermal conductivity by introducing (1) nonlinear effect [9–12], for example, temperature-dependent thermal conductivity like phase change; or (2) dynamic modulation [13–15], for example, by tuning the thermal conductivity dynamically; or (3) structure perturbation [16], by patterning the material to create a metamaterial for phonon or electrons. However, the proposed approaches focus on breaking the reciprocity of electron or phonon transport and still leave the polariton transport reciprocal.

As a hybrid oscillation of electromagnetic waves and charged particles, polaritons have recently been shown to be the potentially dominant heat carriers in materials, especially for nanostructures where the phonon thermal conductivity is suppressed as compared to their bulk counterparts [17,18] as the structures become increasingly miniaturized. Polaritons can also assist ultrafast heat transfer due to their high group velocity [19,20]. In particular, surface plasmon/phonon polaritons have emerged as a promising avenue to enhance thermal conductivity in thin-film and nanowire structures [17,18,20–30]. For instance, studies have revealed that the surface phonon polaritons in ultrathin SiO_2 film can contribute as much thermal conductivity as phonons [21]. It has also been experimentally shown that surface phonon polaritons can significantly improve the thermal transport in nanowire structures [17].

In traditional reciprocal systems, the polaritons exhibit symmetric dispersion relations due to reciprocity, leading to symmetric heat transport. However, recent advancements in nonreciprocal photonics indicate that the reciprocity of polaritons can be broken in nonreciprocal materials, such as magneto-optical systems and magnetic Weyl semimetals [31–34]. These nonreciprocal polaritons have been exploited for achieving thermal radiation that violates the traditional Kirchhoff's law of thermal radiation [31,33,35–41]. Despite significant progress in leveraging nonreciprocal materials for thermal radiation, their potential to enable asymmetric thermal conductivity remains unclear.

In this work, we explore the possibility of achieving nonreciprocal thermal conductivity by exploiting the asymmetric polaritons inherent in nonreciprocal materials. We show that when the reciprocity of the polaritons is broken, the asymmetric dispersions can result in a spectral thermal conductivity that is direction dependent. We discuss the necessary conditions under which nonreciprocal thermal conductivity can be achieved. As examples, we showcase the nonreciprocal thermal conductivity in structures consisting of two types of model materials, magneto-optical materials and Weyl semimetals, where both materials support nonreciprocal surface plasmon polaritons (SPPs). The approaches and discussions are applicable to other polaritons as well.

To calculate the spectral thermal conductivity of SPPs, we employ a framework based on the Boltzmann transport equation under the relaxation time approximation. This method allows a direct evaluation of thermal transport contributions arising from polaritons. The thermal conductivity of SPPs, k_{SPP}, can be obtained by integrating the spectral thermal

*Contact author: bzhao8@uh.edu

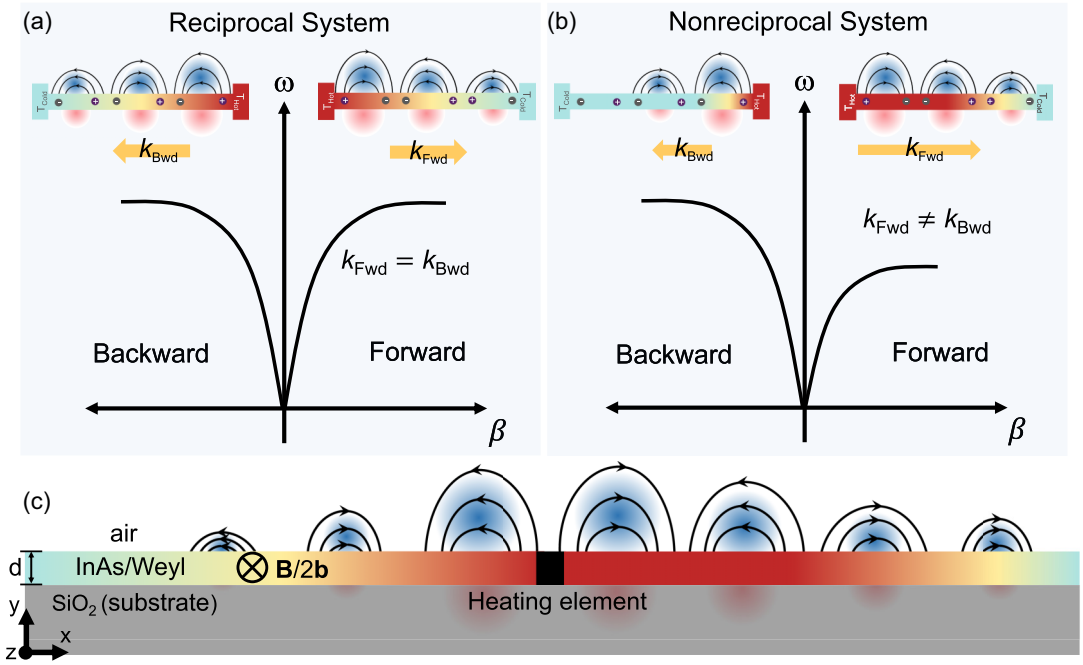

FIG. 1. The concept of nonreciprocal polariton thermal conductivity. (a) Symmetric dispersion in reciprocal systems leads to symmetric heat conductivity. (b) Asymmetric dispersion in a nonreciprocal system leads to asymmetric and nonreciprocal conductivity. The polariton dispersions are for illustration. (c) The schematic of the system studied in this work. A thin layer of nonreciprocal materials (InAs or Weyl semimetals) on a SiO_2 substrate. The black square represents a heating element. When the system is heated, the heat conducted by the polaritons from the source differs in magnitude between the forward and backward directions. The magnetic field for the InAs (**B**) and the momentum separation of Weyl cones, 2**b**, for the Weyl semimetal are both along the $-z$ direction.

conductivity k_ω[21]:

$$k_{\mathrm{SPP}} = \frac{1}{4\pi d}\int_0^\infty k_\omega d\omega = \frac{1}{4\pi d}\int_0^\infty \hbar\omega\Lambda_{\mathrm{eff}}\beta_{\mathrm{R}}\frac{df_0}{dT}d\omega, \quad (1)$$

where $\hbar$ is the reduced Planck constant, ω is the angular frequency, d is the thickness of the material, $\Lambda_{\mathrm{eff}}(\omega)$ is the effective propagation length of SPPs, $\beta_{\mathrm{R}}(\omega)$ is the real part of the wave vector of SPPs, β, and f_0 is the Bose-Einstein distribution function. In this work, we set the temperature as 300 K for all calculations. The effective propagation length, Λ_{eff}, incorporates both the intrinsic propagation properties of the SPPs and the geometrical constraint of the system. It is determined using Matthiessen's rule

$$\Lambda_{\mathrm{eff}}^{-1} = \Lambda^{-1} + r^{-1}. \quad (2)$$

Here, Λ is the intrinsic propagation length of the SPPs, which is determined by the imaginary part of β as $\Lambda = [2\,\mathrm{Im}(\beta)]^{-1}$, and r is the lateral dimension of the sample, representing the maximum length over which SPPs propagate. This equation states that $\Lambda_{\mathrm{eff}} \leqslant r$ and, therefore, ensures that the propagation distance of the polaritons is limited by the real lateral dimension of the sample. Here we assume $r = 30$ mm, a scale for practical devices that is used in previous experimental studies. We note that the k_{SPP} computed using Eq. (1) only considers the contribution of polaritons, which is the focus of this work. The contributions of other carriers should be added when the total conductivity is of interest.

To solve for the spectral k_{SPP}, it is essential to first solve the dispersion relation of the structure supporting SPPs. In reciprocal materials, solving the dispersion relation yields symmetric wave vectors, i.e., $\beta_{\mathrm{Bwd}}(\omega) = \beta_{\mathrm{Fwd}}(\omega)$, for waves propagating towards opposite directions, where Fwd and Bwd are used to indicate the forward and backward directions, respectively. This is true even in anisotropic materials such as hyperbolic materials [21,42,43] since they are all reciprocal. Consequently, the polariton thermal conductivities are equal for both directions ($k_{\mathrm{Bwd}} = k_{\mathrm{Fwd}}$), resulting in reciprocal thermal transport [Fig. 1(a)]. For nonreciprocal materials, the dispersion relation becomes asymmetric, i.e., $\beta_{\mathrm{Bwd}}(\omega) \neq \beta_{\mathrm{Fwd}}(\omega)$, leading to nonreciprocal polariton thermal conductivity ($k_{\mathrm{Bwd}} \neq k_{\mathrm{Fwd}}$), as indicated also in Eq. (1). Therefore, the heat conduction exhibits a difference depending on the direction, as indicated in Fig. 1.

To achieve this nonreciprocal behavior, we employ thin layers of nonreciprocal materials. These materials induce asymmetric SPP propagation through different mechanisms. We begin by introducing Indium Arsenide (InAs) as a nonreciprocal material in our system. InAs is a widely used magneto-optical material for achieving nonreciprocal thermal radiation [31,34,39,44]. The nonreciprocal properties of InAs can be activated by applying an external magnetic field along the z direction, which corresponds to the Voigt configuration [31]. Under this condition, the permittivity tensor for InAs becomes asymmetric and can be represented as [31]

$$\bar{\bar{\varepsilon}} = \begin{bmatrix} \varepsilon_{xx} & i\eta & 0 \\ -i\eta & \varepsilon_{yy} & 0 \\ 0 & 0 & \varepsilon_{zz} \end{bmatrix}, \quad (3)$$

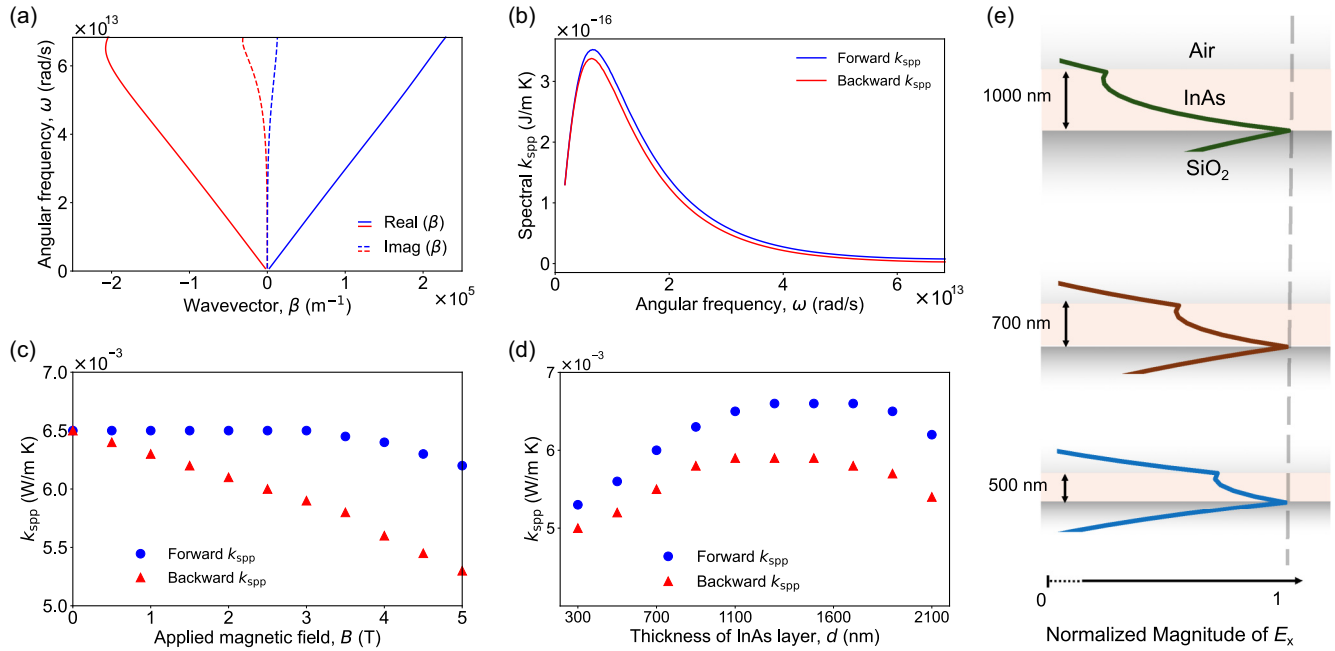

FIG. 2. (a) The dispersion relation of the SPPs for an InAs thin film on SiO_2 and (b) the corresponding spectral conductivity when $B = 3$ T and the thickness of the InAs layer is 1 μm. (c) The polariton thermal conductivity for the same structure when different magnetic fields are applied. (d) The polariton thermal conductivity for different thicknesses of the InAs layer on SiO_2 when $B = 3$ T. (e) Modal profile of SPPs when the InAs film thickness is (from the top to the bottom) 1000, 700, and 500 nm, respectively.

where

$$\varepsilon_{xx} = \varepsilon_{yy} = \varepsilon_d = \varepsilon_\infty - \frac{\omega_p^2(\omega + i\Gamma)}{\omega\left[(\omega + i\Gamma)^2 - \omega_c^2\right]}, \tag{4}$$

$$\eta = \frac{\omega_p^2\omega_c}{\omega\left[(\omega + i\Gamma)^2 - \omega_c^2\right]}, \tag{5}$$

$$\varepsilon_{zz} = \varepsilon_\infty - \frac{\omega_p^2}{\omega(\omega + i\Gamma)}. \tag{6}$$

In the above equations, ε_∞ is the high-frequency permittivity; Γ is the damping rate; $\omega_p = \sqrt{n_e e^2/(m^*\varepsilon_0)}$ is the plasma frequency, where n_e is the carrier concentration, e is the elementary charge, m^* is the effective electron mass, and ε_0 is the vacuum permittivity; and $\omega_c = eB/m^*$ is the cyclotron frequency, with **B** being the applied magnetic field.

We start by solving the dispersion relation of the system shown in Fig. 1(c), a system with a thin film of InAs on a substrate. The dispersion of the SPPs for such a system is given by [45]

$$\tan(\kappa_d d) = \frac{\varepsilon_d\kappa_d\left(\frac{\gamma_{\text{air}}}{\varepsilon_{\text{air}}} + \frac{\gamma_s}{\varepsilon_s}\right)}{\varepsilon_d k_0^2 - \beta^2 - \eta_d\beta\left(\frac{\gamma_{\text{air}}}{\varepsilon_{\text{air}}} - \frac{\gamma_s}{\varepsilon_s}\right) - \left(\varepsilon_d^2 - \eta_d^2\right)\frac{\gamma_{\text{air}}}{\varepsilon_{\text{air}}}\frac{\gamma_s}{\varepsilon_s}}. \tag{7}$$

$\gamma_{\text{air}} = \sqrt{\beta^2 - k_0^2}$, where we assume the medium above the structure is air with $\varepsilon_{\text{air}} = 1$, $\kappa_d = \sqrt{\frac{k_0^2(\varepsilon_d^2 - \eta_d^2)}{\varepsilon_d} - \beta^2}$, and $\gamma_s = \sqrt{\beta^2 - k_0^2\varepsilon_s}$ with ε_s being the permittivity of the substrate. $k_0 = \omega/c$ is the wave vector in the free space, where c is the speed of light. We use SiO_2 as the substrate beneath the nonreciprocal material. As indicated by the above equation, the solution of β is sensitive to its sign, which causes the nonreciprocal dispersion of the polaritons. Therefore, we note that it is critical to make sure the nonreciprocal material is surrounded by an asymmetric dielectric environment such that the term $\gamma_{\text{air}}/\varepsilon_{\text{air}} - \gamma_s/\varepsilon_s$ can remain nonzero. Otherwise, for example, if the substrate is air, the same as the medium above the structure, then $\gamma_{\text{air}}/\varepsilon_{\text{air}} - \gamma_s/\varepsilon_s = 0$ and the solution of Eq. (7) becomes symmetric and reciprocal, despite that the system contains nonreciprocal materials. This highlights the importance of breaking the geometric symmetry for achieving nonreciprocal k_{SPP}. SiO_2 is chosen as the substrate due to its relatively low thermal conductivity of approximately 1.4 W/m K. One can further suspend the film to minimize the conduction from the substrate. The low thermal conductivity of the substrate helps to better highlight the contrast between the left and right thermal conductivities resulting from the SPPs. We solve Eq. (7) using the local minima detection method.

By applying a magnetic field, the dispersions for the forward and backward propagating polaritons become different, as shown in Fig. 2(a). In Fig. 2(b), we show the spectral range within which the spectral polariton thermal conductivity is prominent. We focus on the symmetric branch (long range) of the SPP dispersion, whose contribution to heat conduction is dominant, while the antisymmetric branch (short range) is neglected due to its negligible influence on thermal conductivity. In the Supplemental Material [46], the propagation length, Λ, and also Λ_{eff} are plotted. From these plots, it can be seen that the frequency range of strong spectral k_{SPP} is primarily governed by the propagation length. The high-frequency behavior of k_{SPP} can be understood by rewriting Eq. (1) as $k_{\text{SPP}} = \frac{1}{4\pi d}\int_0^\infty \hbar\omega\Lambda_{\text{eff}}\beta_{\text{R}}\frac{e^{(\hbar\omega/k_BT)}}{(e^{(\hbar\omega/k_BT)}-1)^2}\frac{\hbar\omega}{k_BT^2}d\omega.\Lambda_{\text{eff}}$ gradually

decreases as the frequency increases as shown in Fig. 5 of the Supplemental Material [46]. In the frequency range where the propagation length is long, the real part of the propagation constant β_R increases approximately linearly with respect to the light line, i.e., $\beta_R \sim \omega/c$. Therefore, even without considering the decrease of Λ_{eff} as ω, the ω-dependent term can be simplified as $\sim \frac{(\frac{\hbar\omega}{k_B T})^3}{e^{(\hbar\omega/k_B T)}}$, which approaches zero as ω increases. Therefore, the spectral conductivity gradually decreases as the frequency increases.

Figure 2(c) shows the dependence of k_{SPP} on the external magnetic field. When $B = 0$ T, the system is reciprocal and the forward and backward k_{SPP} overlap. As B increases, the nonreciprocal effect becomes stronger and the contrast between the forward and backward SPPs increases, manifesting as an increasing difference between the corresponding k_{SPP}.

Figure 2(d) shows the dependence of k_{SPP} on the thickness of the InAs layer d when $B = 3$ T. As d increases, k_{SPP} initially increases as well since a thicker layer allows for a longer propagation length for SPPs (see Supplemental Material [46]). On the other hand, as d becomes larger, the $\frac{1}{d}$ factor in Eq. (1) starts to dominate the effect, resulting in a decreasing k_{SPP}. As a result, there exists an optimal thickness—around 1500 nm—at which k_{SPP} reaches its maximum for both forward and backward directions.

The nonreciprocal response of the system is essentially provided by the InAs region. Therefore, the conductivity contrast can be enhanced if the overall field strength in the InAs is stronger. For the system considered here, one can enhance the field strength in the InAs film by increasing its thickness. We solve the modal profile of the SPPs for systems with different InAs thickness, as shown in Fig. 2(e). When the InAs layer becomes thicker, the evanescent wave spans more volume of the region, yielding a larger conductivity contrast as d increases, as seen in Fig. 2(d).

The loss of the SPPs in InAs results in a relatively short propagation length for the nonreciprocal polaritons as shown in the Supplemental Material [46]. Therefore, the nonreciprocal conductivity contrast is on the order of 0.01 W/m K. Materials that can support longer-propagating SPPs could be used to enhance the nonreciprocal contrast. Meanwhile, the necessity of an external magnetic field may introduce some practical challenges [47] in miniaturized systems. For these reasons, we consider an architecture that uses Weyl semimetal as the nonreciprocal material. As a class of topological materials, magnetic Weyl semimetals inherently break time-reversal symmetry, leading to nonreciprocal behavior [33]. Unlike magneto-optical materials that require an external magnetic field to induce nonreciprocity, the nonreciprocal effects in magnetic Weyl semimetals arise intrinsically without the need for an external field. The momentum separation of the Weyl cones, denoted as $2\mathbf{b}$, functions analogously to an applied magnetic field in magneto-optical systems. Weyl semimetals have attracted considerable attention in recent years, not only in theoretical studies but also through research on real materials. The literature shows that Weyl behavior can be realized in experimentally accessible systems. These studies highlight both the scientific importance of Weyl semimetals and their potential for practical applications, since their distinctive properties can be realized and controlled in real material platforms [48–51]. Without loss of generality, we consider a scenario where $\mathbf{b}$ is oriented along the z direction. In this case the permittivity has the same format as Eq. (3), where

$$\eta = \frac{be^2}{2\pi^2\hbar\omega}. \tag{8}$$

When $b \neq 0$, $\bar{\bar{\varepsilon}}$ becomes asymmetric, leading to the breaking of reciprocity. The diagonal element is given by $\varepsilon_{xx} = \varepsilon_{yy} = \varepsilon_{zz} = \varepsilon_b + i\frac{\sigma}{\omega\varepsilon_0}$, where ε_b represents the background permittivity, and σ denotes the bulk conductivity, which is derived from [33]

$$\begin{aligned}\sigma = {} & \frac{\varepsilon_0 r_s g E_F}{6\hbar}\Omega G\left(\frac{E_F\Omega}{2}\right) \\ & + i\frac{\varepsilon_0 r_s g E_F}{6\pi\hbar}\left\{\frac{4}{\Omega}\left[1+\frac{\pi^2}{3}\left(\frac{k_B T}{E_F}\right)^2\right]\right. \\ & \left. + 8\Omega\int_0^{\xi_c}\frac{G(E_F\xi)-G\left(\frac{E_F\Omega}{2}\right)}{\Omega^2-4\xi^2}\xi\, d\xi\right\}.\end{aligned} \tag{9}$$

Here, $r_s = e^2/(4\pi\varepsilon_0\hbar v_F)$ represents the effective fine-structure constant, where $\hbar$ is the reduced Planck constant and v_F is the Fermi velocity. The normalized complex frequency is given by $\Omega = \hbar(\omega + i\tau^{-1})/E_F$, where τ^{-1} is the scattering rate, E_F is the Fermi level, and T is the temperature, assumed to be 300 K in this study. The function $G(E) = n(-E) - n(E)$, where $n(E)$ is the Fermi-Dirac distribution function, g is the number of Weyl points, and k_B is the Boltzmann constant. The normalized cutoff energy is defined as $\xi_c = E_C/E_F$, with E_C being the cutoff energy beyond which the band dispersion ceases to be linear. The values of the parameters are all the same as in Ref. [33].

Based on Eq. (7), we solve the dispersion relation of SPPs for a thin layer of Weyl semimetal on a SiO_2. The dispersion exhibits a similar nonreciprocal behavior as displayed in Fig. 3(a). The corresponding spectral polariton thermal conductivity is shown in Fig. 3(b). As compared to the InAs cases, the spectral range where the conductivity is strong is much broader since the propagation length is significantly longer in the Weyl system, as shown in Fig. 5 in the Supplemental Material [46]. A small peak around 9.5×10^{13} rad/s is caused by the epsilon near zero (ENZ) point of SiO_2, where the real part of its dielectric function (ε_{xx}) crosses zero. The inset in Fig. 3(a) reveals the oscillatory behavior around the ENZ point of SiO_2. Figure 3(c) shows the dependence of the k_{SPP} on the thickness of the Weyl semimetal layer. It follows the same physics and trend shown in Fig. 2(d) as the thickness of the Weyl layer increases. As compared to the InAs system, the nonreciprocal contrast of the conductivity is significantly enhanced by more than 1 order of magnitude, and the strong contrast is obtained without an external magnetic field, paving the way for direct experimental demonstrations.

In the above discussions we focus on the asymmetric polariton thermal conductivity in nonreciprocal materials.

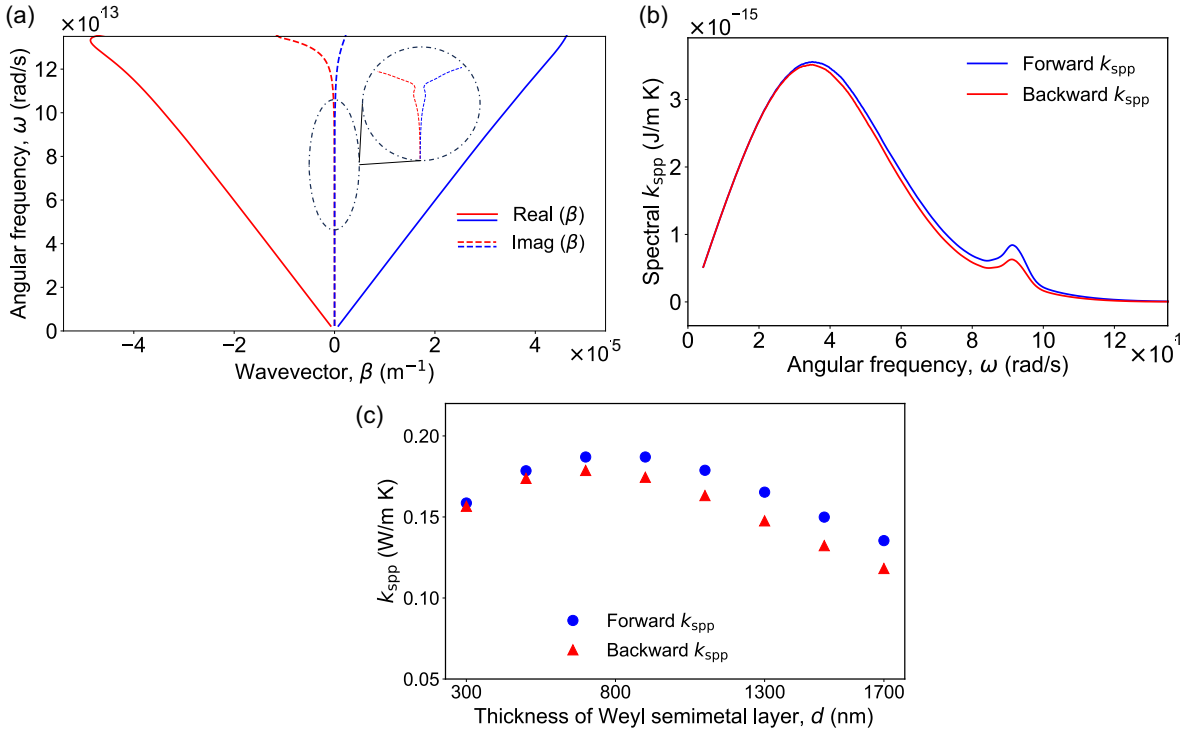

FIG. 3. (a) The dispersion relation for Weyl semimetal thin layer on SiO_2 and (b) the corresponding spectral thermal conductivity, when the thickness of the Weyl layer is 700 nm. (c) The polariton thermal conductivity for different thicknesses of the Weyl semimetal layer on SiO_2.

Leveraging the nonreciprocal polaritons in these materials, one can in fact also create asymmetric thermal conductivity even in reciprocal materials through evanescent wave coupling by controlling the dielectric environment the material is within. To demonstrate the idea, as a baseline, we revisit the work in Ref. [18], where a thin Ti layer on a SiO_2 substrate—both reciprocal materials—is shown to exhibit enhanced Ti thermal conductivity via SPPs. In that system, the forward and backward SPP thermal conductivities are identical. We use the same geometry as Ref. [18] (with $r = 28$ mm), but replace the SiO_2 substrate with InAs, as shown in the inset of Fig. 4(a). When $B = 0$ T, InAs behaves as a reciprocal material, and the system remains symmetric with the forward and backward k_{SPP} overlapping. When $B = 3$ T, we introduce a nonreciprocal material in the dielectric environment of the Ti film. Through near-field coupling, the SPPs in the Ti layer become nonreciprocal, resulting in different forward and backward k_{SPP} in Ti as shown in Fig. 4(a).

The overall trend of k_{SPP} as the thickness of the Ti layer [Fig. 4(a)] is similar to the above two cases. The SPP propagation length for the forward and the backward SPPs at different Ti film thicknesses is shown in Fig. 4(b). By decreasing the thickness of the Ti film, the imaginary part of the wave vector of SPPs increases, leading to shorter propagation lengths. The $\frac{1}{d}$ factor, on the other hand, increases. Therefore, one can expect a Ti film thickness at which the thermal conductivity maximizes, which is around 65 nm for the geometry considered here. On the other side, as the Ti layer becomes thinner, the contribution of polariton-enhanced heat transport to the total thermal conductivity increases. Since this polariton contribution is the sole source of asymmetry in the thermal conductivity, selecting a Ti thickness for which the polariton contribution is significant is crucial in order to achieve the maximum asymmetric thermal conductivity, which also makes the experimental observation more feasible.

Figure 4(c) compares the forward and backward spectral k_{SPP} for several Ti thicknesses. The spectral conductivity peak gradually shifts to higher frequency as the Ti film becomes thicker. Since β_R decreases as the film thickness increases (see Supplemental Material [46]), the fact that the conductivity peaks blueshift as the thickness of the film increases highlights the effect of the increased propagation length towards higher frequencies on the conductivity.

Similar to the previous cases, the contrast between the forward and backward k_{SPP} can be enhanced with a stronger magnetic field. For instance, when $B = 3$ T and the Ti layer thickness is 50 nm, the forward and backward k_{SPP} are 1.79 and 1.76 W/m K, respectively. Increasing the magnetic field to 5 T results in forward and backward k_{SPP} values of 1.80 and 1.74 W/m K, respectively, nearly doubling the contrast.

However, in contrast to previous systems where the nonreciprocal contrast of the conductivity increases as the film thickness increases [Figs. 2(d) and 3(c)], in the current architecture, the contrast increases as the Ti film thickness decreases, as shown in Fig. 4(a). This is caused by the fact that the evanescent wave in the InAs substrate becomes stronger when we have a thinner film. In Figs. 4(d) and 4(e) we illustrate this point using the modal profile of the SPPs at $\omega = 0.21 \times 10^{14}$ and 1.88×10^{14} rad/s, respectively. We show these two cases since the real part of the permittivity of InAs becomes positive when $\omega > 0.77 \times 10^{14}$ rad/s. The SPP profile resembles that of a single-interface SPP in Fig. 4(d), where a thinner Ti film results in a stronger evanescent wave component in the InAs substrate. For the case shown in

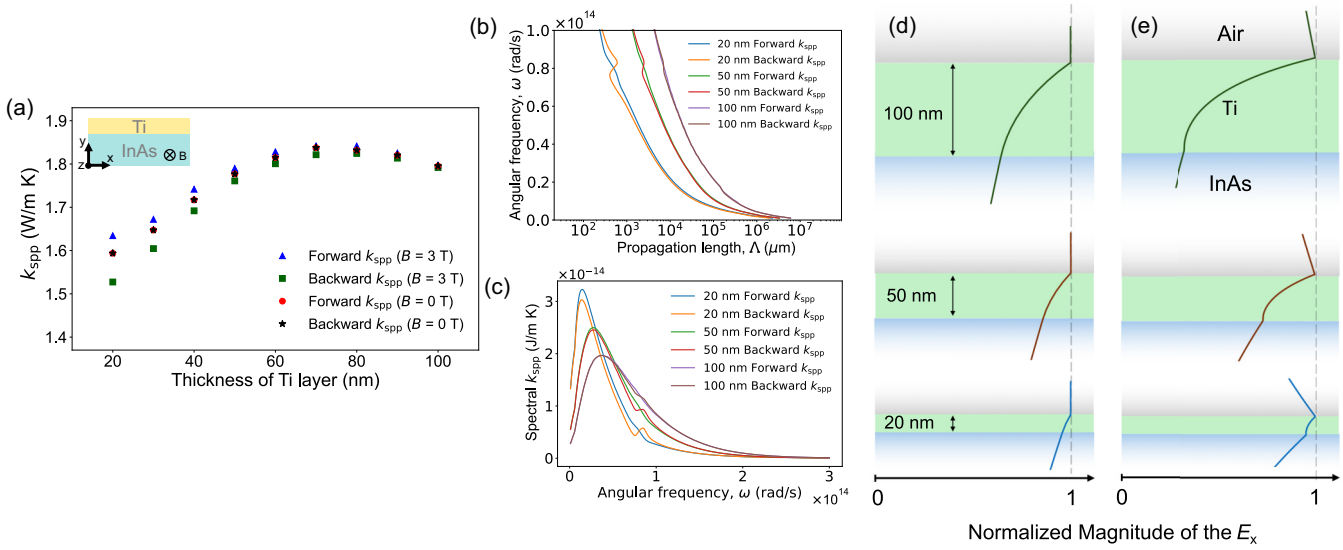

FIG. 4. (a) Polariton thermal conductivity of a Ti thin layer on InAs when the lateral dimension of the sample is 28 mm, corresponding to Ref. [18], for different thicknesses of Ti layer and different magnetic fields. (b) The SPP propagation length for different thicknesses of Ti. (c) The forward and backward spectral k_{SPP} for different thicknesses of the Ti layer. (d) and (e) The modal profile of the SPPs for the studied system for different thicknesses (marked in the figures) at (d) 0.21×10^{14} rad/s and (e) 1.88×10^{14} rad/s.

Fig. 4(e), the SPPs resemble the profile of a symmetric SPP when the Ti film is surrounded by the same dielectric on both sides. The other mode that resembles the antisymmetric SPP contributes negligibly to k_{SPP} due to its significantly shorter propagation length. For this case, the evanescent wave components in the InAs are still stronger as the thickness of the Ti film decreases. Therefore, it is critical to ensure the nonreciprocal material experiences a large portion of the polariton field for a strong contrast in the conductivity.

Conclusion. In conclusion, we demonstrate that nonreciprocal polaritons can mediate direction-dependent thermal conductivity in nanoscale systems, establishing a mechanism for asymmetric heat transport. By exploiting the field-induced or intrinsic time-reversal symmetry-breaking effects in magneto-optical InAs and magnetic Weyl semimetals, we show that polaritons can acquire asymmetric dispersion that leads to nonreciprocal thermal conduction without relying on nonlinearity or temporal modulation in the systems studied in Figs. 2 and 3. The underlying physics can still be observed and exploited in other structures in a similar manner. Through near-field coupling, this nonreciprocal behavior can be imparted to otherwise reciprocal materials, enabling scalable architectures for directional heat flow. As shown in Fig. 4, the magnitude of the thermal conductivity contrast can reach a level of practical interest, making experimental observation of this phenomenon more accessible. The findings shown in this study extend the concept of nonreciprocity from radiative to conductive regimes and open pathways for realizing solid-state thermal diodes, transistors, and other active components in next-generation thermal management and energy systems.

Acknowledgments. B.Z. thanks Dr. Deyu Li and Dr. Renkun Chen for discussions. The authors acknowledge the support from the National Science Foundation under Grants No. CBET-2314210 and No. CBET-2440814. The authors also acknowledge the support from the Research Computing Data Core at the University of Houston for assistance with the calculations carried out in this work.

Data availability. The data that support the findings of this article are not publicly available. The data are available from the authors upon reasonable request.

[1] B. Li, L. Wang, and G. Casati, Thermal diode: Rectification of heat flux, Phys. Rev. Lett. **93**, 184301 (2004).
[2] C. W. Chang, D. Okawa, A. Majumdar, and A. Zettl, Solid-state thermal rectifier, Science **314**, 1121 (2006).
[3] L. Wang and B. Li, Thermal logic gates: Computation with phonons, Phys. Rev. Lett. **99**, 177208 (2007).
[4] L. Wang and B. Li, Thermal memory: A storage of phononic information, Phys. Rev. Lett. **101**, 267203 (2008).
[5] F. Giazotto and M. J. Martínez-Pérez, The Josephson heat interferometer, Nature (London) **492**, 401 (2012).
[6] G. Wehmeyer, T. Yabuki, C. Monachon, J. Wu, and C. Dames, Thermal diodes, regulators, and switches: Physical mechanisms and potential applications, Appl. Phys. Rev. **4**, 041304 (2017).
[7] M. Y. Wong, C. Y. Tso, T. C. Ho, and H. H. Lee, A review of state of the art thermal diodes and their potential applications, Int. J. Heat Mass Transfer **164**, 120607 (2021).
[8] B. Jiang, T. Li, and Z. Chen, Anisotropic Klemens model for the thermal conductivity tensor and its size effect, Int. J. Heat Mass Transfer **226**, 125474 (2024).
[9] G. Dai, J. Shang, R. Wang, and J. Huang, Nonlinear thermotics: Nonlinearity enhancement and harmonic generation in thermal metasurfaces, Eur. Phys. J. B **91**, 59 (2018).
[10] Y. Li, J. Li, M. Qi, C.-W. Qiu, and H. Chen, Diffusive nonreciprocity and thermal diode, Phys. Rev. B **103**, 014307 (2021).
[11] D. B. Go and M. Sen, On the condition for thermal rectification using bulk materials, J. Heat Transfer **132**, 124502 (2010).

[12] A. L. Cottrill, S. Wang, A. T. Liu, W.-J. Wang, and M. S. Strano, Dual phase change thermal diodes for enhanced rectification ratios: Theory and experiment, Adv. Energy Mater. **8**, 1702692 (2018).

[13] M. Camacho, B. Edwards, and N. Engheta, Achieving asymmetry and trapping in diffusion with spatiotemporal metamaterials, Nat. Commun. **11**, 3733 (2020).

[14] J. Li *et al.*, Reciprocity of thermal diffusion in time-modulated systems, Nat. Commun. **13**, 167 (2022).

[15] D. Torrent, O. Poncelet, and J.-C. Batsale, Nonreciprocal thermal material by spatiotemporal modulation, Phys. Rev. Lett. **120**, 125501 (2018).

[16] J. Hu, X. Ruan, and Y. P. Chen, Thermal conductivity and thermal rectification in graphene nanoribbons: A molecular dynamics study, Nano Lett. **9**, 2730 (2009).

[17] Z. Pan, G. Lu, X. Li, J. R. McBride, R. Juneja, M. Long, L. Lindsay, J. D. Caldwell, and D. Li, Remarkable heat conduction mediated by non-equilibrium phonon polaritons, Nature (London) **623**, 307 (2023).

[18] D.-m. Kim, S. Choi, J. Cho, M. Lim, and B. J. Lee, Boosting thermal conductivity by surface plasmon polaritons propagating along a thin Ti film, Phys. Rev. Lett. **130**, 176302 (2023).

[19] W. Hutchins, *et al.*, Ultrafast evanescent heat transfer across solid interfaces via hyperbolic phonon–polariton modes in hexagonal boron nitride, Nat. Mater. **24**, 698 (2025).

[20] D. Li, Z. Pan, and J. D. Caldwell, Phonon polariton-mediated heat conduction: Perspectives from recent progress, J. Mater. Res. **39**, 3193 (2024).

[21] D.-Z. A. Chen, A. Narayanaswamy, and G. Chen, Surface phonon-polariton mediated thermal conductivity enhancement of amorphous thin films, Phys. Rev. B **72**, 155435 (2005).

[22] J. Ordonez-Miranda, L. Tranchant, T. Tokunaga, B. Kim, B. Palpant, Y. Chalopin, T. Antoni, and S. Volz, Anomalous thermal conductivity by surface phonon-polaritons of polar nano thin films due to their asymmetric surrounding media, J. Appl. Phys. **113**, 084311 (2013).

[23] J. Ordonez-Miranda, L. Tranchant, B. Kim, Y. Chalopin, T. Antoni, and S. Volz, Quantized thermal conductance of nanowires at room temperature due to Zenneck surface-phonon polaritons, Phys. Rev. Lett. **112**, 055901 (2014).

[24] Y. Guo, S. Tachikawa, S. Volz, M. Nomura, and J. Ordonez-Miranda, Quantum of thermal conductance of nanofilms due to surface-phonon polaritons, Phys. Rev. B **104**, L201407 (2021).

[25] S. Tachikawa, J. Ordonez-Miranda, Y. Wu, L. Jalabert, R. Anufriev, S. Volz, and M. Nomura, In-plane surface phonon-polariton thermal conduction in dielectric multilayer systems, Appl. Phys. Lett. **121**, 202202 (2022).

[26] K. H. Yun, B. J. Lee, and S. H. Lee, Modeling effective thermal conductivity enhanced by surface waves using the Boltzmann transport equation, Sci. Rep. **12**, 15477 (2022).

[27] S. Li and S. Shin, Long-range polaritonic heat conduction in asymmetric surrounding media, J. Appl. Phys. **134**, 055101 (2023).

[28] J. Minyard and T. E. Beechem, Material characteristics governing in-plane phonon-polariton thermal conductance, J. Appl. Phys. **134**, 165102 (2023).

[29] Y. Pei, L. Chen, W. Jeon, Z. Liu, and R. Chen, Low-dimensional heat conduction in surface phonon polariton waveguide, Nat. Commun. **14**, 8242 (2023).

[30] S. Li, J. Wang, Y. Wen, and S. Shin, Long propagating polaritonic heat transfer: Shaping radiation to conduction, ACS Nano **18**, 14779 (2024).

[31] B. Zhao, Y. Shi, J. Wang, Z. Zhao, N. Zhao, and S. Fan, Near-complete violation of Kirchhoff's law of thermal radiation with a 0.3 T magnetic field, Opt. Lett. **44**, 4203 (2019).

[32] S. J. Ghalekohneh, B. Do, T. Adebiyi, B. Zhao, and R. Zhang, Automated design of nonreciprocal thermal emitters via Bayesian optimization, J. Quant. Spectrosc. Radiat. Transfer **331**, 109260 (2025).

[33] B. Zhao, C. Guo, C. A. Garcia, P. Narang, and S. Fan, Axion-field-enabled nonreciprocal thermal radiation in Weyl semimetals, Nano Lett. **20**, 1923 (2020).

[34] B. Nabavi, S. Jafari Ghalekohneh, K. J. Shayegan, E. J. Tervo, H. Atwater, and B. Zhao, High-temperature strong nonreciprocal thermal radiation from semiconductors, ACS Photonics **12**, 2767 (2025).

[35] L. Zhu and S. Fan, Near-complete violation of detailed balance in thermal radiation, Phys. Rev. B **90**, 220301(R) (2014).

[36] Y. Tsurimaki, X. Qian, S. Pajovic, F. Han, M. Li, and G. Chen, Large nonreciprocal absorption and emission of radiation in type-I Weyl semimetals with time reversal symmetry breaking, Phys. Rev. B **101**, 165426 (2020).

[37] S. Pajovic, Y. Tsurimaki, X. Qian, and G. Chen, Intrinsic nonreciprocal reflection and violation of Kirchhoff's law of radiation in planar type-I magnetic Weyl semimetal surfaces, Phys. Rev. B **102**, 165417 (2020).

[38] T. Liu, C. Guo, W. Li, and S. Fan, Thermal photonics with broken symmetries, eLight **2**, 25 (2022).

[39] K. J. Shayegan, S. Biswas, B. Zhao, S. Fan, and H. A. Atwater, Direct observation of the violation of Kirchhoff's law of thermal radiation, Nat. Photon. **17**, 891 (2023).

[40] M. F. Picardi, V. I. Moerbeek, M. Pascale, and G. T. Papadakis, Nonreciprocity in transmission mode with planar structures for arbitrarily polarized light, Opt. Mater. Express **14**, 2201 (2024).

[41] S. Yang, M. Liu, C. Zhao, S. Fan, and C.-W. Qiu, Nonreciprocal thermal photonics, Nat. Photon. **18**, 412 (2024).

[42] J. Ordonez-Miranda, Y. Wu, M. Nomura, and S. Volz, Near-isotropic polariton heat transport along a polar anisotropic nanofilm, iScience **25**, 104857 (2022).

[43] Y. Guo, J. Ordonez-Miranda, Y. Wu, and S. Volz, Quantifying phonon and polariton heat conduction along polar dielectric nanofilms, J. Appl. Phys. **136**, 044303 (2024).

[44] K. J. Shayegan, B. Zhao, Y. Kim, S. Fan, and H. A. Atwater, Nonreciprocal infrared absorption via resonant magneto-optical coupling to InAs, Sci. Adv. **8**, eabm4308 (2022).

[45] M. Liu, S. Xia, W. Wan, J. Qin, H. Li, C. Zhao, L. Bi, and C.-W. Qiu, Broadband mid-infrared non-reciprocal absorption using magnetized gradient epsilon-near-zero thin films, Nat. Mater. **22**, 1196 (2023).

[46] See Supplemental Material at http://link.aps.org/supplemental/10.1103/pplf-ytqm for the propagation length of the air/(InAs or Weyl)/SiO_2 system and the dispersion of the SPPs in the air/Ti/InAs system.

[47] L. Bi, J. Hu, P. Jiang, D. H. Kim, G. F. Dionne, L. C. Kimerling, and C. Ross, On-chip optical isolation in monolithically integrated non-reciprocal optical resonators, Nat. Photon. **5**, 758 (2011).

[48] N. P. Armitage, E. J. Mele, and A. Vishwanath, Weyl and Dirac semimetals in three-dimensional solids, Rev. Mod. Phys. **90**, 015001 (2018).

[49] L.-L. Wang, N. H. Jo, B. Kuthanazhi, Y. Wu, R. J. McQueeney, A. Kaminski, and P. C. Canfield, Single pair of Weyl fermions in the half-metallic semimetal $EuCd_2As_2$, Phys. Rev. B **99**, 245147 (2019).

[50] B. A. Bernevig, C. Felser, and H. Beidenkopf, Progress and prospects in magnetic topological materials, Nature (London) **603**, 41 (2022).

[51] H. Ness, I. A. Leahy, A. D. Rice, D. Pashov, K. Alberi, and M. van Schilfgaarde, Doping topological Dirac semimetal with magnetic impurities: Electronic structure of Mn-doped Cd_3As_2, Phys. Rev. Res. **7**, 033261 (2025).